Mechanist Model for Contact Between Rough Surfaces

Anil Misra

▶ **To cite this version:**

Anil Misra. Mechanist Model for Contact Between Rough Surfaces. 2011. hal-00555924

HAL Id: hal-00555924
https://hal.science/hal-00555924

Preprint submitted on 14 Jan 2011

HAL is a multi-disciplinary open access archive for the deposit and dissemination of scientific research documents, whether they are published or not. The documents may come from teaching and research institutions in France or abroad, or from public or private research centers.

L'archive ouverte pluridisciplinaire **HAL**, est destinée au dépôt et à la diffusion de documents scientifiques de niveau recherche, publiés ou non, émanant des établissements d'enseignement et de recherche français ou étrangers, des laboratoires publics ou privés.

MECHANISTIC MODEL FOR CONTACT BETWEEN ROUGH SURFACES

By Anil Misra,[1] Associate Member, ASCE

ABSTRACT: Interactions at interfaces play a pivotal role in the mechanics of particulate and fractured material. This paper focusses on the mathematical modeling of force-deformation behavior of interface between two rough surfaces. A mechanistic approach is adopted wherein the overall behavior of rough interfaces are considered via interaction of asperities on the interface. The interacting asperities are modeled using the Hertz-Mindlin contact theory. Both elastic deformation and frictional sliding are accounted at asperity contacts. The topography of the interface is represented via statistical distributions of asperity contact orientations, asperity heights, and asperity curvature. A modified spherical harmonic expansion is introduced to model the asperity contact orientation distribution. The resulting interface force-deformation model is used to predict the normal and the shear stiffness of rough interfaces. The model is verified via comparison with experimental data culled from the literature.

INTRODUCTION

Materials with discrete, particulate nature occur in a variety of engineering applications, such as powder precursors in materials processing and soils, gravel, and jointed rocks in geomechanics. To consider the effect of the discrete nature of these materials on their mechanical behavior, there has been a growing interest, in developing models of such materials from a particle or block interaction standpoint (Misra 1995). The essence of these efforts has been to develop models that predict the bulk, overall mechanical behavior of particulate materials based on the geometric arrangement of constituent particles/blocks and the particle mechanical and geometrical properties. In these modeling methodologies, the behavior of the interfaces between particles/blocks has a pivotal role.

In the field of interface behavior, the study of effects produced by mutual compression of nonconforming elastic bodies was pioneered by Hertz, who considered the case in which forces were normal to a topographically smooth interface surface. Although topographically smooth particles provide an important starting point in the study of interface behavior, they seldom represent realistic situations. The mechanical behavior of particle interfaces is more complex and influenced by a great variety of factors, such as the particle elastic properties, size, shape, friction, surface adhesion, surface topography, and presence of liquid at interface. A number of studies have been published, since the pioneering work by Hertz, that have aimed to address more realistic interfaces (Johnson 1985; Hills et al. 1992). In this work, we present an interface model that describes the force-deformation behavior of rough interfaces. The intent of this paper is to present expressions for interface stiffness in directions normal as well as tangential to the interface. The expressions are derived accounting for the tangential sliding at asperity contacts. These expressions are presented in a form suitable for use in the modeling of particulate materials.

BACKGROUND

At the interface of rough surfaces, the actual contact is between the asperities on the surfaces. Thus the force-deformation behavior of the interface is determined by the behavior of asperity contacts as recognized in the paper by Archard (1957), which dealt with the elastic deformation and friction laws of a mating rough surface and rigid plane. Along these lines, considering asperity contacts to be Hertzian in nature and using gaussian distributions of surface heights, Greenwood and Williamson (1966) derived a model for the mechanical behavior of a rough surface mating a rigid plane. The Greenwood-Williamson model was subsequently extended by Greenwood and coworkers to numerically study the behavior of mating rough surfaces under normal loads [see Hills et al. (1992), chapter 14]. The normal contact of rough surfaces has been widely studied (see, e.g., Swan 1983; Brown and Scholz 1985, 1986). Models of mating rough surfaces under normal loads have also been developed by treating the asperities to be elliptical paraboloids (Bush et al. 1975; O'Callaghan and Cameron 1976). These models have been used to simulate isotropic as well as anisotropic interface surfaces by accounting for aspect ratios and principal axis orientations of elliptical paraboloid asperities (Bush et al. 1978; McCool and Gassel 1981; McCool 1986). The plasticity of asperity contacts has been considered in the context of Greenwood-Williamson approach (see Chang et al. 1987). Further, the analysis of Greenwood and Williamson (1966) has been extended to study the normal and shear behavior of mating rough surfaces under elastic deformation of asperity contacts (Yamada et al. 1978; Swan and Jongqi 1985; Yoshioka and Scholz 1989). More recent studies have considered the sliding at asperity contacts with the aim of obtaining friction behavior of mating rough surfaces (Boitnott et al. 1992; Ford 1994). From a numerical simulation viewpoint, finite-element models have been used to simulate the behavior of rough surfaces (Kikuchi and Oden 1988; Kucharski et al. 1994). In addition, micromechanism-inspired approaches have been developed for cracked concrete (Divakar and Fafitis 1992) and phenomenological approaches have been developed for geological interfaces, such as rock joints (see e.g., Desai and Nagaraj 1988; Qui et al. 1993).

In the present paper, we develop a micromechanical methodology to derive force-deformation relationships of mating rough surfaces by including the effect of sliding at inclined asperity contacts. To this end, a directional distribution function of asperity contacts at the interface surface is developed and incorporated in the derivation. In the discussion that follows, we first present a description of the modeling methodology as it pertains to the characterization of interface geometry, the force-deformation relationship at an asperity contact, and the consequent derivation of the interface force-deformation relationship. The derived interface force-deformation relationship is subsequently used to study interface behavior for a variety of asperity contact behavior and loading conditions. The predictions of the derived model are compared with experimental data from the literature.

MODEL DESCRIPTION

At the interface of rough particles the actual contact is between the asperities on particle surface. Thus the force-defor-

[1]Assoc. Prof. of Civ. Engrg., Univ. of Missouri–Kansas City, 5100 Rockhill Rd., Kansas City, MO 64110.

Note. Associate Editor: Robert Y. Liang. Discussion open until October 1, 1997. To extend the closing date one month, a written request must be filed with the ASCE Manager of Journals. The manuscript for this paper was submitted for review and possible publication on July 31, 1995. This paper is part of the ***Journal of Engineering Mechanics***, Vol. 123, No. 5, May, 1997. ©ASCE, ISSN 0733-9399/97/0005-0475–0484/ $4.00 + $.50 per page. Paper No. 11284.

mation behavior of the surface is determined by the behavior of individual asperities. From the view point of studying mechanics of interfaces, information is required about the geometry and the mechanical behavior of asperity contact. To this end, in the subsequent sections we describe the approach adopted in the present work for characterizing: (1) the asperity geometry by examining the interface geometry; (2) the mechanical interaction at an asperity contact; and (3) the overall mechanical interaction of an interface.

Interface Geometry

The roughness of a surface may be considered in terms of statistics of parameters that describe its deviation from a mean plane surface. These parameters are typically taken to be the surface height, the surface slope, and the curvature (Nayak 1971). In general, these parameters are scale-dependent, and therefore, will depend on the resolution of the measuring device (Singer and Pollock 1992). The fractal nature of surfaces have been considered in order to describe the scale dependency of these parameters (Majumdar and Bhusan 1991). For a given resolution, the surface characteristics may be reasonably described via statistics of surface height, curvature, and surface slope. In view of this, we consider statistical distributions of asperity heights, asperity curvatures, and asperity contact orientations, to describe the interface topography for developing model of interface mechanics. While, the forms of distribution functions of asperity heights and asperity curvatures are known based on topography measurements of rough surfaces, a spherical-harmonics–based distribution function of asperity contact orientation is introduced here for the first time.

Asperity Height

Topography measurements on rough surfaces generally provide data on asperity heights and asperity curvature. From the view point of modeling interface behavior, the asperity height distribution of a composite topography of mating surfaces has been found to be more applicable (Brown and Scholz 1985). Along this line, it is convenient to interpret the asperity height with reference to the highest peak of the composite topography, such that the asperity height r is same as the overlap of the mating surfaces under a given interface force or displacement. Given that the total number of asperities per unit area at an interface is N, the quantity $NH(r)dr$ denotes the number of asperity contacts in the interval represented by r and $r + dr$. Thus, the total number of asperity contacts under a given interface force or displacement is obtained as

$$N_r = \int_0^r NH(r)\, dr \tag{1}$$

The experimental measurements of topography suggests a skewed distribution for asperity heights and several statistical distributions, such as chi-square distribution and gamma distribution have been used to model rough surfaces (see Adler and Firman 1981; Yoshioka and Scholz 1989). In this paper we use a gamma distribution for simplicity; however, it is noteworthy that a chi-square distribution provides a more versatile representation. For a gamma distribution of asperity heights, the density function $H(r)$ is expressed as

$$H(r) = \frac{r^{\alpha} e^{-r/\beta}}{\Gamma(\alpha + 1)\beta^{\alpha+1}} \quad (0 < r < \infty,\ \alpha > -1,\ \beta > 0) \tag{2}$$

where α and β = parameters related to the mean and variance of the asperity heights as follows:

$$\text{mean: } r_m = \beta(\alpha + 1); \quad \text{variance: } r_0^2 = \beta^2(\alpha + 1) \tag{3a,b}$$

Fig. 1 illustrates the distribution of asperity heights for smooth and rough surfaces based on data from Yoshioka and Scholz (1989) on Westerly granite. The measured asperity height distribution is denoted by solid dots and the best fit gamma distribution is represented by solid curve with following parameters: $\alpha = 3.82$ and $\beta = 1.15$ for smooth interface, and $\alpha = 6.14$ and $\beta = 3.52$ for rough interface.

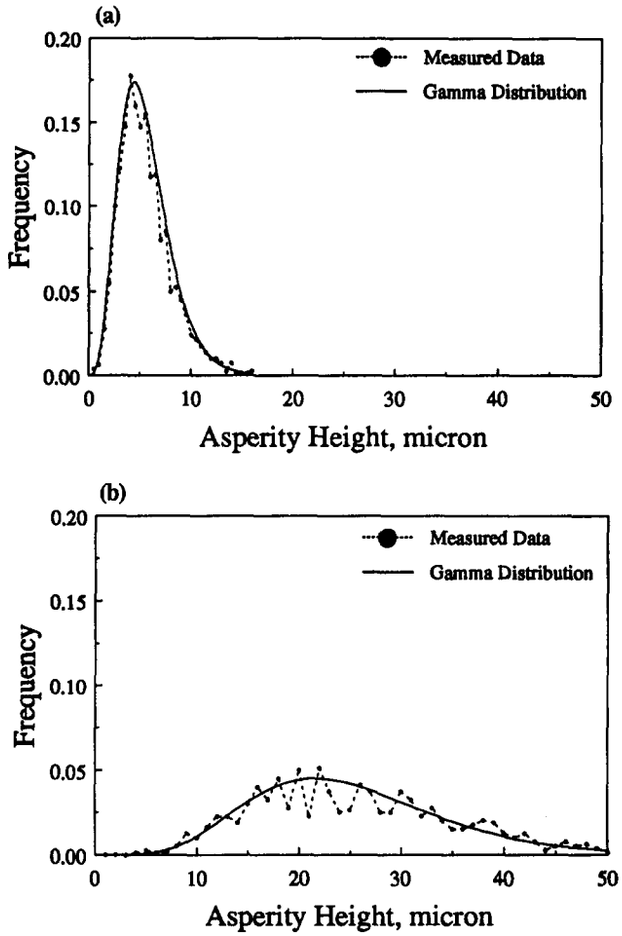

FIG. 1. Asperity Height Distributions for: (a) Smooth Interface, (b) Rough Interface

Asperity Radius of Curvature

Experimental measurements also suggest that the radius of curvature of asperities is best represented by a non-Gaussian distribution, such as a gamma or a chi-square distribution (Adler and Firman 1981). It is noted, however, that the measurements reported by Yoshioka and Scholz (1989) indicate a narrow distribution implying an almost uniform distribution of asperity radius of curvature. Also, the mean radius of curvature is found to be larger for smooth surfaces than for rough surfaces. Given that $G(R)$ denotes the probability density of asperity curvature R, the number of asperity contacts N_R with radius of curvature in the interval R and $R + dR$ is given by

$$N_R = N_r G(R)\, dR \tag{4}$$

Asperity Contact Orientation

The distribution of asperity contact orientation requires a three-dimensional density function. Spherical harmonics expansion have been successfully used to represent such density functions (Chang and Misra 1989). Here, we use a modified form of spherical harmonics expansion to represent the asperity contact distribution for interfaces ranging from smooth to rough. As illustrated in Fig. 2, in comparison to rough inter-

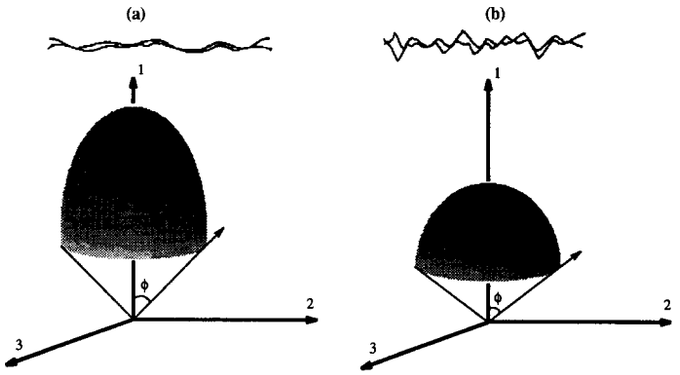

FIG. 2. Schematic Depiction of Asperity Contact Orientations for: (a) Smooth Interface; (b) Rough Interfaces

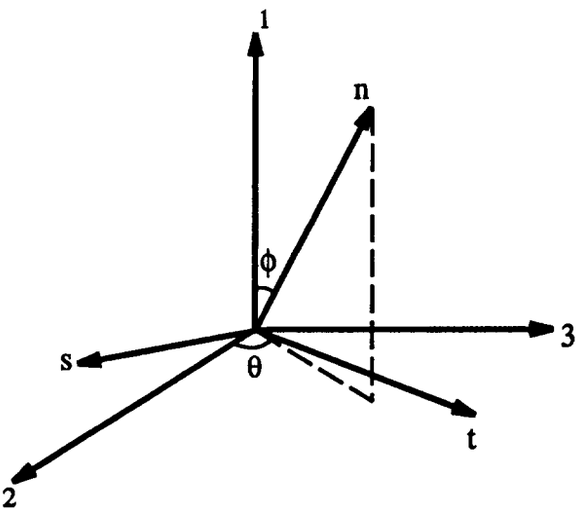

FIG. 3. Coordinate System

faces, for smooth interfaces the asperity contacts have a greater tendency to concentrate in the direction normal to the interface. In particular, a perfectly smooth interface will have a single contact in the normal direction, while a very rough surface is likely to have asperity contact orientations in all directions of the half-space. To represent these various interfaces, the spherical harmonics expansions are written for the conical domain given by $0 \leq \phi \leq \pi/2a$ and $0 \leq \theta \leq 2\pi$, where $a \geq 1$. In this paper, the density function, $\xi(\Omega)$, of the directional distribution of asperity contacts is expressed by a truncated spherical harmonics expansion consisting of lower order terms as follows:

$$\xi(\Omega) = \frac{a \sin a\phi}{2\pi \sin \phi}\left[1 + \frac{b}{4}(3 \cos 2a\phi + 1) + 3c \sin^2 a\phi \cos 2\theta\right]$$

$$\left(0 \leq \phi \leq \frac{\pi}{2a};\quad 0 \leq \theta \leq 2\pi;\quad a \geq 1\right) \tag{5}$$

where angles θ and ϕ are defined in Fig. 3. Higher-order terms may be included to represent more complex orientation distributions; however, the terms included in (5) are adequate to model cross-anisotropy of an interface. It is straightforward to show that the density function, $\xi(\Omega)$, satisfies the condition

$$\int_0^{2\pi}\int_0^{\pi/2a} \xi(\phi, \theta)\sin \phi \, d\phi \, d\theta = 1 \tag{6}$$

and that $N_r\xi(\Omega)\, d\Omega$ denotes that number of asperity contacts N_Ω in the interval represented by solid angles Ω and $\Omega + d\Omega$, that is

$$N_\Omega = N_r\xi(\Omega)\, d\Omega \tag{7}$$

In (5), the parameter a models the influence of interface roughness on contact orientation and the parameters b and c, describe the directional nature of roughness on the interface surface. The parameters a and b are related to the average asperity contact orientation, calculated as the expectation $E[\phi] = \int \phi\xi(\Omega)\, d\Omega$, and the variance of asperity contact orientation, calculated as the expectation $E[(\phi - E[\phi])^2] = \int(\phi - E[\phi])^2\xi(\Omega)\, d\Omega$, as follows

$$E[\phi] = \frac{6-b}{6a} \text{ and } E[(\phi - E[\phi])^2] = \frac{36\pi - 108 + 20b - 6b\pi - b^2}{36a^2} \tag{8}$$

It is noted that as the parameter α increases, the contact distribution concentrates toward the direction normal to the interface. In the limit $a \to \infty$, the contact distribution concentrates to a single contact normal to the interface, i.e., $E[\phi] = 0$, representing a perfectly smooth interface. It is noteworthy that the density function, $\xi(\Omega)$, behaves like a delta function in the limit $a \to \infty$, thus, it appropriately represents a concentrated contact orientation normal to the interface.

Interactions of Asperities

The interaction at an asperity contact is assumed to be a Hertz-Mindlin–type contact of topographically smooth interface, wherein, the asperity contact is represented by interaction between rigid bodies connected via springs and sliders. Under an arbitrary motion of interacting surfaces, the relative motion δ_j^c at an asperity contact may be decomposed, in general, into an elastic part δ_j^{ce} and an inelastic part δ_j^{cp}, such that

$$\delta_j^c = \delta_j^{ce} + \delta_j^{cp} \tag{9}$$

Considering a smooth sliding at the asperity, the inelastic part of relative motion, δ_j^{cp}, is expressed by

$$\delta_j^{cp} = \gamma^c\zeta_j^c \tag{10}$$

where γ = magnitude of the inelastic motion; and ζ_j^c = sliding direction.

The force generated by the relative motion at an asperity contact is related via the asperity spring constant, K_{ij}^c, as follows:

$$f_i^c = K_{ij}^c\delta_j^{ce} \tag{11}$$

or, from (9) and (10)

$$f_i^c = K_{ij}^c(\delta_j^c - \gamma^c\zeta_j^c) \tag{12}$$

At an asperity contact, sliding is governed by Amonton-Coulomb's friction law, expressed by the following inequality:

$$f_i^c q_i^c \leq 0 \tag{13}$$

$$\text{where} \quad q_i^c = \zeta_i^c + \mu n_i^c \tag{14}$$

where μ = asperity friction coefficient; and n_i^c = vector normal to the asperity contact. It follows from (12) and (13), that at the point of impending sliding at an asperity contact

$$K_{ij}^c(\delta_j^c - \gamma^c\zeta_j^c)q_i^c = 0 \tag{15}$$

which yields the following expression for the magnitude of inelastic motion, γ^c, in terms of the relative motion, δ_j^c

$$\gamma^c = (M^c K_{ij}^c q_i^c)\delta_j^c \tag{16}$$

where the scalar M^c is given by

$$M^c = (K_{ij}^c\zeta_j^c q_i^c)^{-1} \tag{17}$$

Thus, (12) and (16) lead to the following relationship be-

tween the force and relative motion at a sliding asperity contact:

$$f_i^c = K_{ir}^c(\delta_{rj} - M^c K_{sj}^c q_s^c \zeta_r^c)\delta_j^c \tag{18}$$

where δ_{rj}(=1 for $r = j$; =0 for $r \neq j$) is the Kronecker delta.

Interactions of Interface

Considering the equilibrium of two interacting particles, the overall force F_i at the interface is the summation of the forces developed at asperities f_i^c, that is

$$F_i = \sum_c f_i^c \tag{19}$$

For a large number of asperity contacts, the summation can be replaced by the following integration accounting for the distributions of asperity heights, asperity contact orientations and asperity radius of curvature

$$F_i = N \int_r \int_\Omega \int_R f_i^c G(R)\xi(\Omega)H(r)\, dR\, d\Omega\, dr \tag{20}$$

where overall force F_i is given as force per unit area, since N is measured per unit area of an interface.

For further consideration, it is reasonable to assume that the relative motion at an asperity, δ_j^c, is same as the relative motion of the interface δ_j. For a given asperity contact orientation, the relative motion, $\delta_j^c = \delta_j$, may result in sliding, separation or in elastic deformation of the contact. Eq. (18) gives the asperity contact forces, f_i^c, for contacts that are undergoing elastic and sliding deformation. Thus, using (18) and (20) and appropriately accounting for the separating asperity contacts, the relationship between the overall force F_i at the interface and the relative motion δ_j may be written as

$$F_i = C_{ij}\delta_j = [C_{ij}^e - C_{ij}^p]\delta_j \tag{21}$$

where the superscripts e and p refer to the elastic and inelastic part of the interface stiffness tensor, C_{ij}.

The elastic part, C_{ij}^e, is independent of the interface loading condition, given by

$$C_{ij}^e = N \int_r \int_\Omega \int_R K_{ij}^c G(R)\xi(\Omega)H(r)\, dR\, d\Omega\, dr \tag{22}$$

where the integration is performed over all the asperity contacts at the interface. On the other hand, the inelastic part depends on the interface loading condition. The inelastic part of the interface stiffness tensor, C_{ij}^p, is given by

$$C_{ij}^p = N \int_{r^s} \int_{\Omega^s} \int_{R^s} M^c K_{ik}^c \zeta_k^c K_{mj}^c q_m^c G(R)\xi(\Omega)H(r)\, dR\, d\Omega\, dr + N \int_{r^d} \int_{\Omega^d} \int_{R^d} K_{ij}^c G(R)\xi(\Omega)H(r)\, dR\, d\Omega\, dr \tag{23}$$

where the integration is performed over the domain of sliding asperity contacts denoted by superscript s and separated asperity contacts denoted by superscript d.

INTERFACE BEHAVIOR

Since the domain of sliding and separated asperity contacts is not always known a priori, numerical effort is typically required to evaluate the integrals in (22) and (23) to obtain the interface stiffness. Nevertheless, under certain simple conditions the integrals in (22) and (23) may be evaluated in closed forms to obtain analytical expressions of interface stiffness. For the subsequent derivation, it is convenient to express the asperity stiffness tensor, K_{ij}^c, in terms of asperity stiffness that describe the behavior along the direction of the normal and tangent to asperity contact, such that

$$K_{ij}^c = K_n^c n_i^c n_j^c + K_s^c(\mathbf{s}_i^c \mathbf{s}_j^c + \mathbf{t}_i^c t_j^c) \tag{24}$$

where K_n and K_s denote asperity stiffness along the normal and tangential direction of the asperity. It is assumed that stiffness terms that cross-link normal and shear behavior are negligible. The unit vector $\mathbf{n}$ is normal to the asperity contact surface and vectors $\mathbf{s}$ and $\mathbf{t}$ are arbitrarily chosen on the plane tangential to the asperity contact surface, such that $\mathbf{nst}$ forms a local cartesian coordinate system, as illustrated in Fig. 3. The vectors $\mathbf{n}$, $\mathbf{s}$, and $\mathbf{t}$ used in this paper are given by

$$\mathbf{n} = \langle \cos\phi,\ \sin\phi\cos\theta,\ \sin\phi\sin\theta \rangle \tag{25a}$$

$$\mathbf{s} = \langle -\sin\phi,\ \cos\phi\cos\theta,\ \cos\phi\sin\theta \rangle \tag{25b}$$

$$\mathbf{t} = \langle 0,\ -\sin\theta,\ \cos\theta \rangle \tag{25c}$$

Elastic Behavior

The elastic part of the interface stiffness may be obtained by integrating (22). For simplicity of derivation, we consider uniform asperity heights and asperity curvature, thus (22) is reduced to

$$C_{ij}^e = N \int_\Omega K_{ij}^c \xi(\Omega)\, d\Omega \quad \text{or} \tag{26}$$

$$C_{ij}^e = N \int_0^{2\pi} \int_0^{\pi/2a} K_{ij}^c \xi(\phi, \theta)\sin\phi\, d\phi\, d\theta \tag{27}$$

TABLE 1. Analytical Expressions for Elastic Interface Stiffness

Parameter number, a (1)	NC_{11} (2)	NC_{22} (3)	NC_{33} (4)
1	$\frac{1}{3}(K_n + 2K_s) + \frac{2b}{15}(K_n - K_s)$	$\frac{1}{3}(K_n + 2K_s) - \frac{b}{15}(K_n - K_s) + \frac{2c}{5}(K_n - K_s)$	$\frac{1}{3}(K_n + 2K_s) - \frac{b}{15}(K_n - K_s) - \frac{2c}{5}(K_n - K_s)$
2	$\frac{1}{4}(3K_n + K_s) + \frac{b}{16}(K_n - K_s)$	$\frac{1}{8}(K_n + 7K_s) - \frac{b}{32}(K_n - K_s) + \frac{5c}{32}(K_n - K_s)$	$\frac{1}{8}(K_n + 7K_s) - \frac{b}{32}(K_n - K_s) - \frac{5c}{32}(K_n - K_s)$
3	$\frac{1}{5}(7K_n - 2K_s) - \frac{3\sqrt{3}}{10}(K_n - K_s) + \frac{(69\sqrt{3} - 72)b}{1{,}540}(K_n - K_s)$	$-\frac{1}{5}(K_n - 6K_s) + \frac{3\sqrt{3}}{20}(K_n - K_s) - \frac{(69\sqrt{3} - 72)b}{3{,}080}(K_n - K_s) + \frac{(531\sqrt{3} - 688)c}{3{,}080}(K_n - K_s)$	$-\frac{1}{5}(K_n - 6K_s) + \frac{3\sqrt{3}}{20}(K_n - K_s) - \frac{(69\sqrt{3} - 72)b}{3{,}080}(K_n - K_s) + \frac{(531\sqrt{3} - 688)c}{3{,}080}(K_n - K_s)$
∞	K_n	K_s	K_s

where the asperity orientation density function $\xi(\Omega)$ is given in (5). Since the general form of the analytical expressions is quite complex, particular expression for roughness parameter $a = 1$, 2, 3, and ∞ are given in Table 1. It is noted that the terms that cross-link the normal and shear stiffness, namely C^e_{ij} $(i \neq j)$, are identically zero.

It is noteworthy that as the parameter a tends toward infinity, i.e., as the asperity contacts tend to align in the vertical direction, the interface stiffness tensor C^e_{ij} becomes proportional to that of a single asperity contact. Given that the asperity contact density $N = 1$ for a topographically smooth interface, the interface stiffness C^e_{ij}, at $a = \infty$, correctly reduces to the interface stiffness of topographically smooth surfaces. The dependency of interface stiffness upon the roughness parameter a is further illustrated in Fig. 4(a,b), in which the normalized normal and shear interface stiffness, i.e., NC_{11}/K_n and NC_{22}/K_s, are plotted for isotropic interface with asperity contact orientation parameters $b = c = 0$. It is seen that the interface stiffness is related to the ratio of asperity normal and tangential stiffness, i.e., K_n/K_s. The interface stiffness is proportional to asperity stiffness for asperity stiffness ratio $K_n/K_s = 1$. It is also observed that the interface stiffness approaches proportionality to asperity stiffness at the roughness parameter $a \approx 6$, which would typically represent an interface with a majority of asperity contact in the vertical direction, such as an interface of gradually undulating surfaces.

The ratio of interface tangential stiffness to normal stiffness also depends on the roughness parameter, a, as illustrated in Fig. 5, in which the ratio C_{22}/C_{11} is plotted versus the roughness parameter a for asperity stiffness ratio $K_s/K_n = 1$, 0.5, and 2. As expected from previous discussion, the interface stiffness

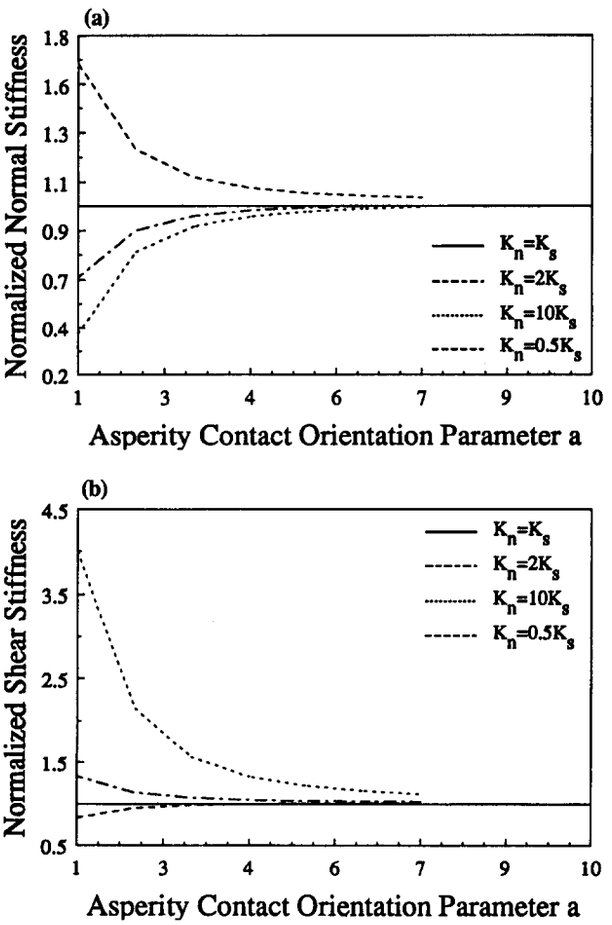

FIG. 4. Dependency of Interface Elastic Stiffness on Asperity Orientation Parameter *a*

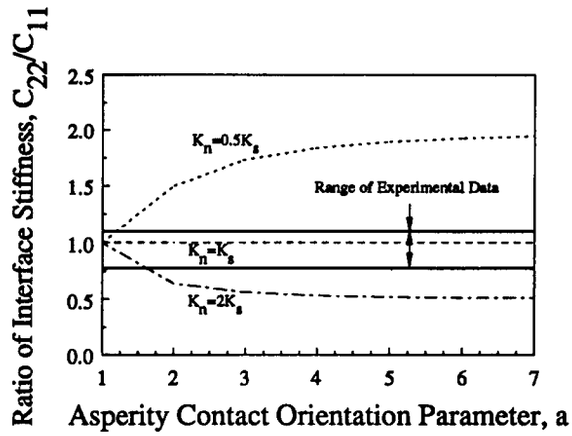

FIG. 5. Ratio of Interface Elastic Tangential Stiffness to Normal Stiffness

ratio becomes asymptotic to the asperity stiffness ratio K_s/K_n as the roughness parameter increases. Experimental results of interface stiffness ratio reported by Krolikowski and Szczepek (1993) are also depicted in Fig. 5. These interface stiffness ratio were obtained by an ultrasonic method for interface of ground quartz samples pressed together at various normal pressures. The ultrasonic method measures the elastic behavior as little inelastic deformations are expected for this method. The measured ratios exhibited no discernible dependence upon the normal pressure and displayed considerable scatter varying from 1.1 to 0.78. Since the roughness parameter is not known for the experimental data, horizontal lines are drawn at ratios 1.1 and 0.78 to indicate the range of measured data. It is also noted that Hertz-Mindlin contact theory for topographically smooth interface predicts the following ratio for elastic contact:

$$\frac{K_s}{K_n} = \frac{2(1 - \nu)}{2 - \nu} \tag{28}$$

yielding an interface stiffness ratio ranging from 1 to 0.67 for Poisson's ratio, ν, ranging from 0 to 0.5.

Inelastic Behavior under Interface Normal Deformation

For normal deformation of an interface such that $\delta_1 = \delta$, $\delta_2 = \delta_3 = 0$, the asperity contacts do not separate. Therefore, the sliding at asperity contacts is the sole contributor to the inelastic part of the stiffness tensor, C^p_{ij}. Under the normal deformation of an interface, the sliding direction at an asperity contact is given by the vector s defined in (25), so that $\zeta^c_j = s^c_j$. In this case, the sliding domain may be denoted by: $0 \leq$

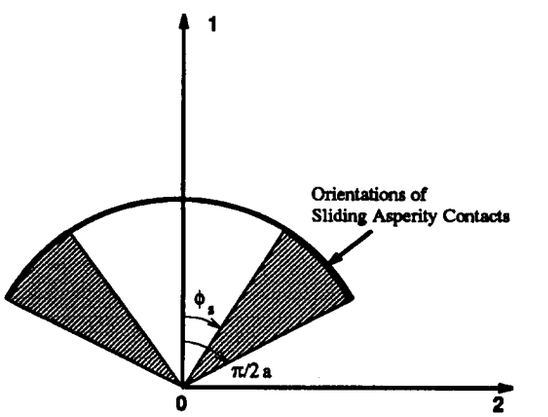

FIG. 6. Orientations of Sliding Asperity Contacts

TABLE 2. Analytical Expressions for Inelastic Interface Stiffness under Normal Deformation

Parameter number, a (1)	NC^p_{11} (2)	$NC^p_{22} = NC^p_{33}$ (3)
1	$\frac{1}{3}\mu K_n(\sin^3\phi_s - 1) + \frac{1}{3}K_s\cos\phi_s(3 - \cos^2\phi_s)$	$\frac{1}{6}\mu K_n(1 - \sin^3\phi_s) + \frac{1}{6}K_s\cos^3\phi_s$
2	$\frac{1}{8}\mu K_n(4\phi_s - \pi - \sin 4\phi_s) + \frac{1}{8}K_s(4\cos 2\phi_s - \cos 4\phi_s - 1)$	$\frac{1}{16}\mu K_n(\pi + \sin 4\phi_s - 4\phi_s) + \frac{1}{16}K_s(4\cos 2\phi_s + \cos 4\phi_s + 1)$
∞	0	K_s

$\theta \le 2\pi$ and $\phi_s \le \phi \le \pi/2a$. That is, the asperity contacts oriented in the directions indicated by the hatched area in Fig. 6, will undergo sliding. Now, considering, for simplicity, the case of uniform asperity heights and asperity curvature, the inelastic part of the interface stiffness tensor C^p_{ij} may be obtained as

$$C^p_{ij} = N\int_{\Omega^*} M^c K^c_{ik}\zeta^c_k K^c_{mj} q^c_m \xi(\Omega)\, d\Omega \quad \text{or} \tag{29}$$

$$C^p_{ij} = N\int_0^{2\pi}\int_{\phi_s}^{\pi/2a} M^c K^c_{ik}\zeta^c_k K^c_{mj} q^c_m \xi(\phi, \theta)\sin\phi\, d\phi\, d\theta \tag{30}$$

where the asperity orientation density function $\xi(\Omega)$ is given in (5).

Linear Asperity Contact Behavior

For linear asperity contact behavior, the asperity stiffness K_n and K_s are constants, independent of asperity force or displacement. Thus, using the Amonton-Coulomb friction law in (13) along with (12), the sliding domain is given by: $0 \le \theta \le 2\pi$ and $\phi_s \le \phi \le \pi/2a$, where

$$\phi_s = \arctan\left(\frac{\mu K_n}{K_s}\right) \tag{31}$$

and μ = asperity friction coefficient. It is noteworthy that sliding at an asperity contact is not only governed by the asperity friction coefficient but also by the ratio of asperity normal and tangential stiffness.

Thus, integrating (30), closed-form expressions for the inelastic part of the interface stiffness may be obtained. For isotropic interfaces, with asperity contact orientation parameter $b = c = 0$, expressions for the inelastic part of interface stiffness are tabulated in Table 2 for roughness parameter $a = 1$, 2, and ∞. It is noted that the cross-linking term that link the shear and normal behaviors are identically zero, i.e., $C^p_{12} = C^p_{13} = C^p_{23} = 0$.

Further, for frictionless asperity contact, i.e., $\mu = 0$ and consequently $\phi_s = 0$, the expressions for the inelastic part of normal stiffness tensor, C^p_{11}, reduce to

$$C^p_{11} = \frac{2K_s}{3}, \quad \text{for } a = 1;\ C^p_{11} = \frac{K_s}{4}, \quad \text{for } a = 2 \tag{32}$$

As expected, for this case, the normal interface stiffness, C_{11}, is independent of asperity shear stiffness K_s, given by

$$C_{11} = \frac{K_n}{3}, \text{ for } a = 1; \quad C_{11} = \frac{3K_n}{4}, \quad \text{for } a = 2 \tag{33}$$

It is also noteworthy that as roughness parameter a tends to infinity the inelastic part of normal interface stiffness, C^p_{11}, vanishes. Thus for roughness parameter $a = \infty$, the normal interface stiffness, C_{11}, is proportional to normal asperity stiffness K_n.

Nonlinear Asperity Contact Behavior

The Hertz-Mindlin contact theory for topographically smooth elastic interface as well as other works on plastic interface, show that the asperity contact stiffness is dependent on contact force or displacement. In this work, we assume that the normal asperity stiffness, K_n, depends on the normal asperity deformation, δ_n, according to the following power law

$$K_n = \lambda K \delta_n^{\eta} \tag{34}$$

where K, λ, and η are constants. Further, for simplicity, the tangential asperity stiffness, K_s, is assumed to be independent of asperity loading conditions in the tangential direction, given by

$$K_s = K\delta_n^{\eta} \tag{35}$$

It is noted, however, that asperity sliding is accounted in accordance with (13) and the sliding domain is given by: $0 \le \theta \le 2\pi$ and $\phi_s \le \phi \le \pi/2a$, where $\phi_s = \arctan(\lambda\mu)$. The asperity stiffness, K_n and K_s, given by (34) and (35), become identical with the Hertz-Mindlin stiffness for contact of topographically smooth spheres when

$$\lambda = \frac{2 - \nu}{2(1 - \nu)}, \quad \eta = \frac{1}{2}, \quad \text{and} \quad K = \frac{G\sqrt{12R}}{2 - \nu} \tag{36}$$

where G = shear modulus; ν = Poisson's ratio, and R = asperity curvature. The exponent η can vary from 0 for perfectly plastic to 1/2 for perfectly elastic behavior at contact of smooth spherical asperities (Johnson 1985). It is noteworthy that the exponent η has a direct influence on the nonlinearity exhibited by the interface. For nonlinear asperity, exact closed-form expressions of the interface stiffness are only possible for exponent $\eta = 1$, however, numerical solutions may be calculated for a variety of asperity nonlinearity. For the subsequent examples, we take constant $K = 1$ MPa $\mu m^{1/2}$, number of asperity contact $N = 1{,}050$ per μm^2 and asperity contact orientation

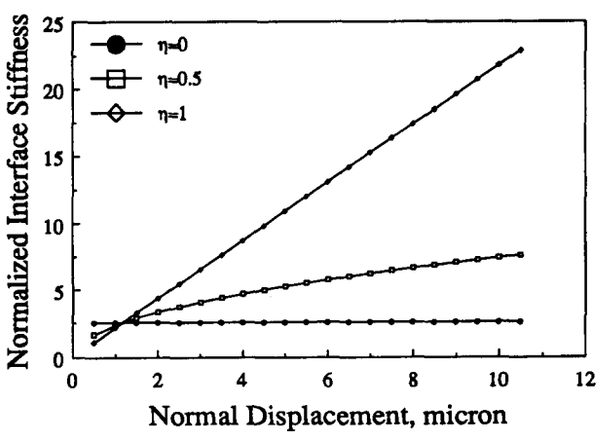

FIG. 7. Effect of Asperity Nonlinearity on Interface Stiffness

parameter $a = 2$ and $b = c = 0$. The asperity contact friction is chosen to be large such that no sliding occurs at the contacts. Fig. 7 illustrates the effect of exponent η on the nonlinear behavior of an interface. For a perfectly plastic asperity contact, i.e., $\eta = 0$, the interface stiffness is independent of loading conditions.

In Fig. 8(a, b) we plot the normalized normal stiffness C_{11}/K_n and shear stiffness C_{22}/K_s versus normal displacement for $\lambda = 0.5$, 1, and 2, and exponent $\eta = 0.5$. It is observed that the normal as well as the shear stiffness vary nonlinearly with normal displacement. A power law fit of the normal and shear stiffness versus normal displacement yields an exponent of 0.5, which varies only slightly with asperity friction coefficient, μ. It is also interesting to note that the normalized normal stiffness is higher for $\lambda = 0.5$ than for $\lambda = 2$. The trend is reversed for the normalized shear stiffness.

For further numerical parametric study, we admit the possibility of formation of new asperity contacts as the interface is loaded. Thus the interface stiffness is obtained from

$$C_{ij}^e = N \int_0^r \int_0^{2\pi} \int_0^{\pi/2a} K_{ij}^c \xi(\phi, \theta) \sin \phi \, d\phi \, d\theta H(r) \, dr \quad (37)$$

and

$$C_{ij}^p = N \int_0^r \int_0^{2\pi} \int_{\Phi_a}^{\pi/2a} M^c K_{ik}^c \zeta_k^c K_{mj}^c q_m^c \xi(\phi, \theta) \sin \phi \, d\phi \, d\theta H(r) \, dr \quad (38)$$

where $H(r)$ = asperity height distribution given by (2); $r = r_o + \delta$; and r_o = asperity overlap at $\delta = 0$. Fig. 9 illustrates the effect of contact formation on the normal stiffness for rough interface described by the following parameters: $\alpha = 6.14$ and $\beta = 3.52$ for asperity distribution, and $a = 2$ for asperity contact orientation. It is found that with new contact formation, the power law dependence of the interface normal stiffness is given by an exponent of 1.2 for $\eta = 0.5$. In contrast, the power law exponent is 0.5, for $\eta = 0.5$, when contact formation is not considered.

The normal displacement versus normal stress curves obtained from the present model are compared in Fig. 10, with the experimental data on interfaces between Westerly granite blocks reported by Yoshioka and Scholz (1989). The calculated curves are given by solid lines while the experimental data are indicated by symbols. The calculated curves were obtained using the following parameters: $\eta = 0.5$, $K = 2.4$ MPa $\mu m^{1/2}$ [using $G = 100$ GPa; $R = 50$ μm; and $\nu = 0$ in (36)], and $\lambda = 0.8$. Asperity orientation parameter $a = 3$ for rough and $a = 6$ for smooth interface. The parameters λ and a are chosen to produce a good fit with the measured data. The initial overlap $r_o = 12$ μm for the rough interface and 2 μm for the smooth interface, which are similar to the initial overlaps reported by Yoshioka and Scholz (1989). The asperity height distributions for the smooth and rough interfaces are given in Fig. 1. The model correctly replicates a stiffer response as well as a greater displacement hardening for smooth interface. The stiffer response and displacement hardening of smooth interface is attributable to primarily two factors: (1) the narrow distribution of asperity heights that results in a rapid increase of the contact area due to the formation of new contacts; and (2) the concentration of asperity contact orientation distribution toward the direction normal to the interface.

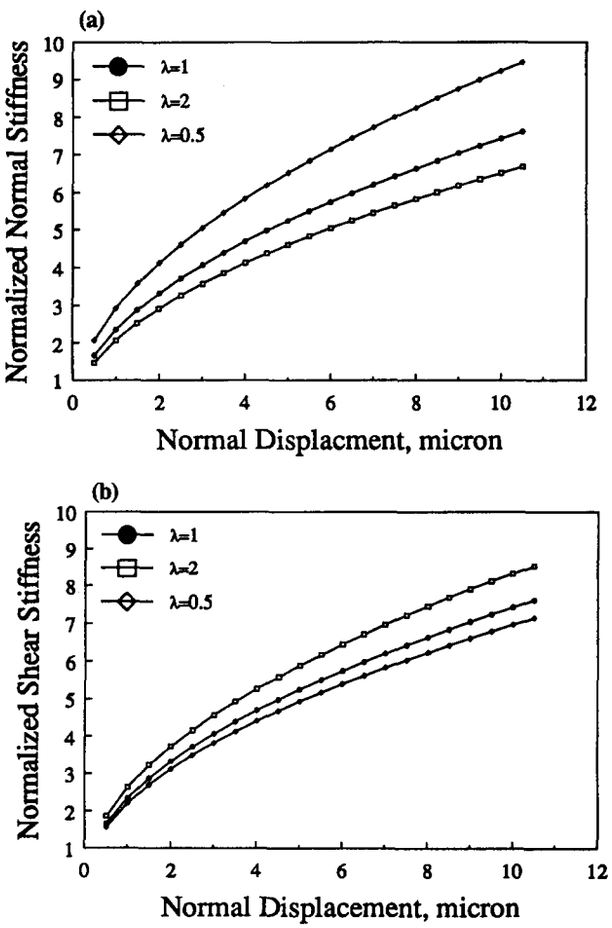

FIG. 8. Effect of Ratio of Asperity Normal to Tangential Stiffness on Interface Stiffness

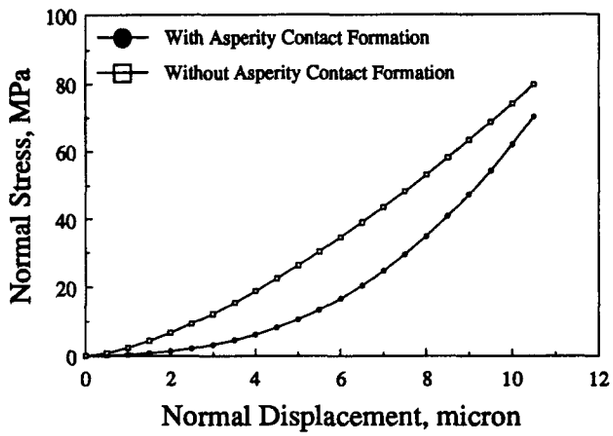

FIG. 9. Effect of Asperity Contact Formation on Interface Normal Stiffness

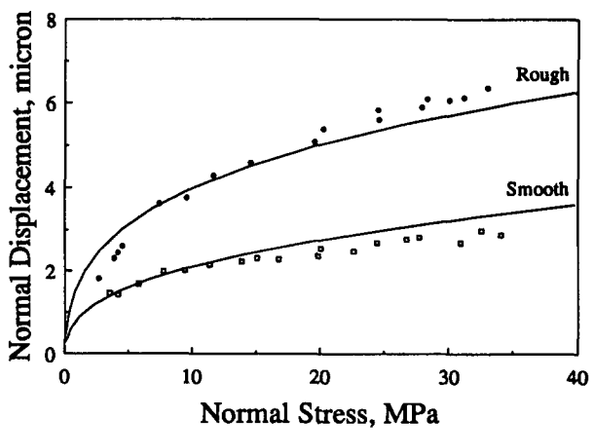

FIG. 10. Comparison of Measured and Predicted Interface Normal Behavior

Experimental measurements also show that the initial shear stiffness increases nonlinearly with normal stress (Yoshioka and Scholz 1989; Jing et al. 1992). In Fig. 11(a, b), we compare the initial shear stiffness calculated with the present model to the experimental data from Yoshioka and Scholz (1989) and Jing et al. (1992), respectively. As in the case of normal stiffness, it is observed from Fig. 11(a), that the smooth interface has a higher initial shear stiffness than the rough interface at a given normal stress. It is also observed that the initial shear stiffness of rough interface exhibits a greater nonlinearity in relation to normal stress than the smooth interface. The nonlinear behavior is attributable to formation of new contacts as the normal stress is increased. Further, in the case of smooth interfaces, a majority of the new contact formation occurs at relatively low normal stresses. Therefore, the nonlinearity of the dependence of initial shear stiffness on normal stress diminishes at higher normal stresses.

From a comparison of Fig. 11(a, b), it is observed that although the measured data has same trends, the values of initial shear stiffness reported by Jing et al. (1992) are considerably smaller than those reported by Yoshioka and Scholz (1989). Interestingly, this is a manifestation of the scale-dependent nature of interface behavior. It is noteworthy that the tests by Jing et al. (1992) were performed using concrete replicas of rock joints. For these interfaces, the number of asperity contacts per unit area are expected to be larger as the sand used for making the concrete replicas have a mean grain radius of 15 mm. Jing et al. (1992) did not report any topography measurements. In the absence of these measurements, for our calculations we use the parameters for smooth interface illustrated in Fig. 1, with the modification that asperity heights and asperity curvature are given in millimeters.

Inelastic Behavior under Interface Shear Deformation

Under shear deformation of an interface, such that $\delta_1 \neq \delta_2 \neq \delta_3 \neq 0$, the asperity contacts can separate as well as slide. Therefore, asperity separation as well as sliding, contribute to the inelastic part of the stiffness tensor, C^p_{ij}. In contrast to the case of normal loading, for shear loading, closed form solutions that give the orientations of sliding and separating asperity contacts are complex and difficult to obtain. Numerically, the asperity separation may be detected by examining the total relative motion in the normal direction of an asperity contact. The sliding of an asperity contact is controlled by Amonton-Coulomb law, as discussed previously, and the sliding occurs along the shear force at the asperity contact. The inelastic part of the interface behavior, in this case, may be obtained by numerically integrating (23). In the examples discussed hereafter, we consider asperity curvature to be uniform.

In Fig. (12), we plot the shear resistance, given by F_1/F_2, versus the shear displacement for asperity orientation parameter a = 2, 3, 6, and 9. The asperity friction coefficient μ is taken to be 0.6 and asperity stiffness assumed to be linear, i.e., $\eta = 0$, $K = 1$ MPa $\mu m^{1/2}$, and $\lambda = 1$. A normal displacement of $\delta_1 = 1$ μm is maintained during the shear loading given by $\delta_2 > 0$ and $\delta_3 = 0$. Although asperity orientation parameter a has small effect upon the initial stiffness, it has a significant effect on the interface frictional resistance. From Fig. 12, it is seen that the interface friction tends toward asperity friction

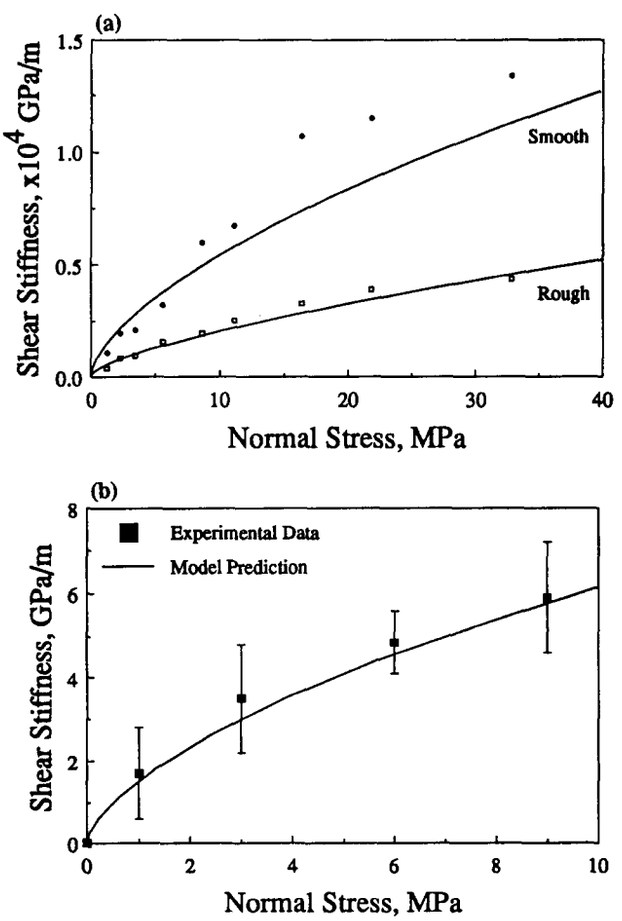

FIG. 11. Comparison of Measured and Predicted Shear Stiffness versus Normal Stress for Data from: (a) Yoshioka and Scholz (1989); (b) Jing et al. 1992

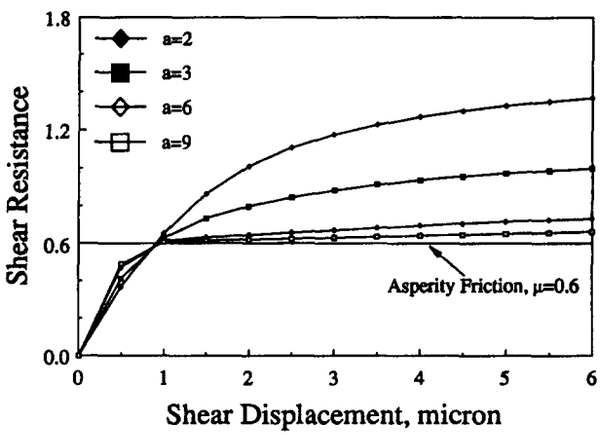

FIG. 12. Effect of Asperity Orientation Parameter *a* on Interface Shear Resistance Behavior

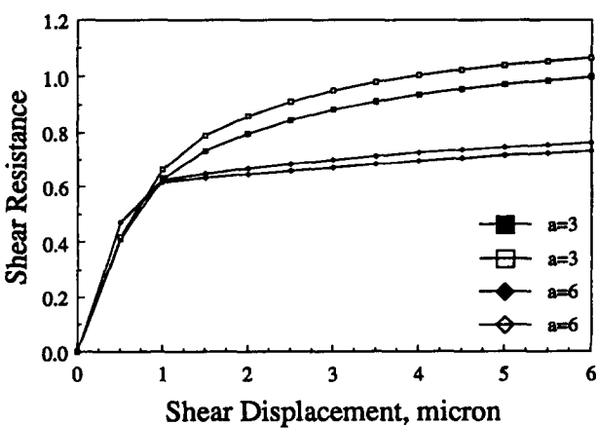

FIG. 13. Effect of Asperity Nonlinearity on Interface Shear Resistance Behavior

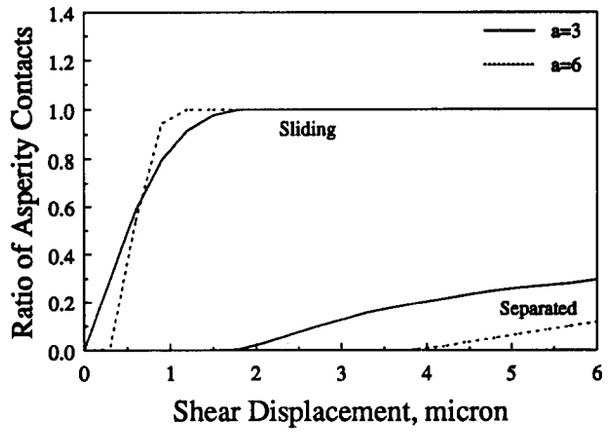

FIG. 14. Evolution of Sliding and Separation of Asperity Contacts with Shear Displacement

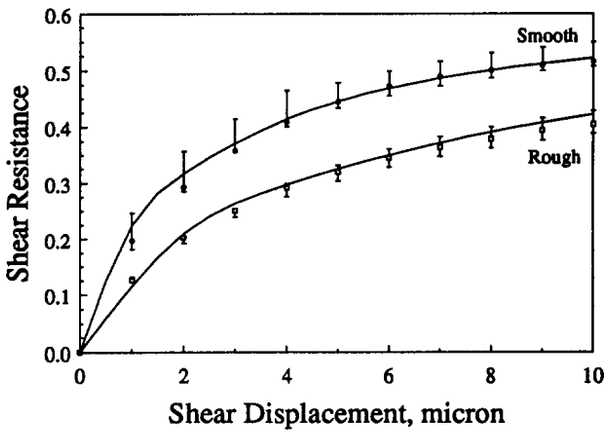

FIG. 15. Comparison of Measured and Predicted Interface Shear Resistance

as a increases. It may be recalled that a higher value of asperity orientation parameter a indicates a smoother interface.

Fig. 13 illustrates the effect of nonlinear asperity stiffness on interface shear resistance. Results for linear asperity stiffness are shown by filled symbols and those for nonlinear asperity ($\eta = 0.5$) by open symbols. It is observed that interface with linear asperity exhibits a lower shear resistance than that with nonlinear asperity stiffness for the same initial normal loading condition. In addition, the effect is more pronounced for a rough surface with $a = 3$, than for a smooth surface with $a = 6$. Similar results are borne out from the simplified formulae of interface friction given by Ford (1994), which show that linear asperity contacts have a lower effect of roughness on shear resistance of an interface than nonlinear asperity contacts.

The evolution of sliding and separation of asperity contacts during shear loading is illustrated in Fig. 14. In comparison to the rough interface ($a = 3$), the sliding at asperity contacts is mobilized at a lower shear displacement and a lower shear resistance for the smooth interface ($a = 6$). The asperity contact separation, on the other hand, commences at a higher shear displacement for the smooth interface. It is noted that for the smooth interface ($a = 6$), a larger number of asperity contacts are inclined in the direction normal to the interface which expedites sliding at shear resistance close to the asperity friction coefficient while retarding the asperity separation. The average asperity inclination, calculated as the expectation $E(\phi) = \int \phi \xi(\Omega)\, d\Omega$, is 10° for $a = 6$ and 19° for $a = 3$.

In the preceding examples, asperity contact formation is not considered and asperity heights are taken to be uniform. To investigate the effect of asperity contact formation and asperity heights, we study the model performance by comparison with experimental results presented by Biegel et al. (1992) on interfaces between Westerly granite blocks. Experimental results show that a smooth interface, with a narrow distribution of asperity heights, exhibits higher shear resistance as well as deformation hardening before interface yield. Here, interface yield is defined as the point at which the interface shear resistance changes drastically. In comparison, a rough interface, with a relatively broad distribution of asperity heights, has a lower shear resistance and deformation hardening. Although the behavior may seem counterintuitive, smooth interfaces exhibit higher shear resistance than rough interfaces because of a larger initial contact area under the same initial normal loading conditions. The present model correctly replicates this trend as illustrated in Fig. 15. The model results were calculated using the following parameters: $\eta = 0.5$, $K = 2.4$ MPa $\mu m^{1/2}$, and $\lambda = 0.8$. Asperity orientation parameter $a = 3$ and asperity friction coefficient $\mu = 0.2$. The initial overlap $r_o = 12$ μm for the rough interface and 2 μm for the smooth interface. The asperity height distributions used in the calculations are given in Fig. 1.

CONCLUDING REMARKS

The main result of this paper is contained in (22) and (23), which give the formulation for stiffness tensor of rough interfaces. The applicability of the derived formulation is demonstrated by parametric studies of elastic and inelastic behavior of interfaces. Comparisons are also made with experiments.

The interface stiffness is modeled by considering the contacts between surface asperities. The composite surface topography of a rough interface is characterized via statistical distributions of asperity heights, asperity curvature and asperity contact orientation. A modified spherical harmonic expansion is introduced to model the asperity contact orientation distribution. Using this orientation distribution, the inelastic sliding and separation of asperity contacts are explicitly incorporated in the model. Since the model directly considers the asperity contact behavior, a variety of asperity conditions, such as plastic flow and adhesion, may be incorporated. It is noted, however, that the formulation does not account for asperity breakages due to ploughing or gouging. It also ignores the presence of debris at the interface.

Interface behavior studied with the derived model show that the roughness of an interface is best characterized by distributions of asperity heights and asperity contact orientations. Closed-form expressions of interface elastic stiffness were obtained which show the variation of the relative effect of asperity normal and tangential stiffness with the interface roughness as described by the asperity contact orientations. These closed form expressions may be used as first approximation of rough interface stiffness in modeling of jointed and granular materials.

Comparison with experimental data suggests that average values of asperity heights and asperity contact orientation may not be sufficient to capture all nuances of interface behavior. Asperity contact formation, as described by asperity height distribution, is important for distinguishing the smooth and rough interface stiffness behavior. Further, the roughness of interface, as described by the asperity contact orientation parameter a, has a significant effect on the friction behavior of interface. It is noteworthy that the present model correctly replicates the deformation hardening exhibited by rough interfaces under going shear.

APPENDIX I. REFERENCES

Adler, R. J., and Firman, D. (1981). "A non-Gaussian model for random surfaces." *Philosophical Trans. of Royal Soc. of London*, London, En-

gland, A303, 433–462.
Archard, J. F. (1957). "Elastic deformation and the laws of friction." *Proc., of Royal Soc. of London*, London, England, A243, 190–205.
Biegel, R. L., Wang, W., Scholz, C. H., Boitnott, G. N., and Yoshioka, N. (1992). "Micromechanics of rock friction 1. Effects of surface roughness of initial friction and slip hardening in Westerly Granite." *J. Geophys. Res.*, 97(B6), 8951–8964.
Boitnott, G. N., Biegel, R. L., Scholz, C. H., Yoshioka, N., and Wang, W. (1992). "Micromechanics of rock friction 2. Quantitative modelling of initial friction with contact theory." *J. Geophys. Res.*, 97(B6), 8965–8978.
Brown, S. R., and Scholz, C. H. (1985). "Closure of random elastic surfaces in contacts." *J. Geophys. Res.*, 90(B7), 5531–5545.
Brown, S. R., and Scholz, C. H. (1986). "Closure of rock joints." *J. Geophys. Res.*, 91(B5), 4939–4948.
Bush, A. W., Gibson, R. D., and Thomas, T. R. (1975). "The elastic contact of a rough surface." *Wear*, 35, 87–111.
Bush, A. W., Gibson, R. D., and Keogh, G. P. (1978). "Strongly anisotropic rough surface." *ASME Paper 78-LUB-16*, Am. Soc. of Mech. Engrs., New York, N.Y.
Chang, C. S., and Misra, A. (1990). "Packing structure and mechanical properties of granulates." *J. Engrg. Mech.*, ASCE, 116(5), 1077–1093.
Chang, W. R., Etsion, I., and Bogy, D. R. (1987). "An elastic-plastic model for the contact of rough surfaces." *J. of Tribology*, 109(1), 257–263.
Desai, C. S., and Nagaraj, B. K. (1988). "Modeling for cyclic normal and shear behavior of interfaces." *J. of Engrg. Mech.*, ASCE, 114(7), 1198–1217.
Divakar, M. P., and Fafitis, A. (1992). "Micromechanics-based constitutive model for interface shear." *J. of Engrg. Mech.*, 118(7), 1317–1337.
Ford, I. J. (1993). "Roughness effect on friction for multi-asperity contact between surfaces." *J. Phys. D: Appl. Phys.*, 26, 2219–2225.
Greenwood, J. A., and Williamson, J. B. P. (1966). "Contact of nominally flat surfaces." *Proc., Royal Soc. of London*, London, England, A295, 300–319.
Hills, D. A., Nowell, D., and Sackfield, A. (1992). *Mechanics of elastic contacts*. Butterworth-Heinemann, Stoneham, Mass.
Jing, L., Nordlund, E., and Stephansson, O. (1992). "An experimental study on the anisotropy and stress-dependency of the strength and deformability of rock joints." *Int. J. Rock Mech. and Min. Sci. and Geomech. Abstracts*, 29(6), 535–542.
Johnson, K. L. (1985). *Contact mechanics*. Cambridge University Press, London, England.
Kikuchi, N., and Oden, J. T. (1988). *Contact problems in elasticity: a study of variational inequalities and finite element methods*. Soc. for Industrial and Appl. Math., Philadelphia, Pa.
Krolikowski, J., and Szczepek, J. (1993). "Assessment of tangential and normal stiffness of contact between rough surfaces using ultrasonic method." *Wear*, 160, 253–258.
Kucharski, S., Klimczak, T., Polijaniuk, A., and Kaczmarek, J. (1994). "Finite-elements model for the contact of rough surfaces." *Wear*, 177, 1–13.
Majumdar, A., and Bhusan, B. (1991). "Fractal model of elastic-plastic contact between rough surfaces." *J. Tribology*, 113(1), 1–11.
McCool, J. I. (1986). "Comparison of models for the contact of rough surfaces." *Wear*, 107, 37–60.
McCool, J. I., and Gassel, S. S. (1981). "The contact of two surfaces having anisotropic roughness geometry." *Energy Technol., Am. Soc. of Lubrication Engrs. Spec. Publ. SP-7*, 29–38.
Misra, A. (1995). "Interfaces in particulate materials." *Mechanics of geomaterial interfaces*, A. P. S. Selavadurai and M. P. Boulon, eds., 513–536, Elsevier Science Publishers BV (North-Holland), Amsterdam, The Netherlands.
Nayak, P. R. (1971). "Random process model of rough surfaces." *J. Lubrication Technol.*, 93, 398–407.
O'Callaghan, M., and Cameron, M. A. (1976). "Static contact under load between nominally flat surfaces in which deformation is purely elastic." *Wear*, 36, 79–97.
Qiu, X., Plesha, M. E., Huang, X., and Haimson, B. C. (1993). "An investigation of the mechanics of rock joints—Part II. Analytical investigation." *Int. J. Rock Mech. and Min. Sci. and Geomech. Abstracts*, 30(3), 271–287.
Singer, I. L., and Pollock, H. M. (1992). *Fundamental of friction: macroscopic and microscopic processes*. Kluwer, Dordrecht, The Netherlands.
Swan, G. (1983). "Determination of stiffness and other joint properties from roughness measurements." *Rock Mech. and Rock Engrg.*, 16, 19–38.
Swan, G., and Jongqi, S. (1985). "Prediction of shear behavior of joints using profiles." *Rock Mech. and Rock Engrg.*, 18, 183–212.
Yamada, K., Takeda, N., Kagami, J., and Naoi, T. (1978). "Mechanisms of elastic contact and friction between rough surfaces." *Wear*, 48, 15–34.
Yoshioka, N., and Scholz, C. H. (1989). "Elastic properties of contacting surfaces under normal and shear loads." *J. Geophys. Res.*, 94(B12), 17,681–17,700.

APPENDIX II. NOTATION

The following symbols are used in this paper:

a, b, c = parameter of $\xi(\Omega)$;
C_{ij} = interface stiffness;
F_i = interface force;
f_i = asperity contact force;
$G(R)$ = asperity curvature distribution function;
$H(r)$ = asperity height distribution function;
K_{ij} = asperity contact stiffness;
N = number of asperity contacts per unit area;
R = asperity curvature;
r = asperity height;
α, β = parameter of $H(r)$;
γ = magnitude of asperity contact inelastic deformation;
δ_i = interface deformation vector;
δ_i^c = asperity contact deformation vector;
θ, ϕ = spherical coordinates;
ζ_i = sliding direction;
$\xi(\Omega)$ = asperity contact orientation distribution; and
Ω = solid angle.